Atmos. Meas. Tech., 5, 2375–2390, 2012
www.atmos-meas-tech.net/5/2375/2012/
doi:10.5194/amt-5-2375-2012

Atmospheric Measurement Techniques

SCIAMACHY WFM-DOAS XCO_2: reduction of scattering related errors

J. Heymann[1], H. Bovensmann[1], M. Buchwitz[1], J. P. Burrows[1], N. M. Deutscher[1], J. Notholt[1], M. Rettinger[2], M. Reuter[1], O. Schneising[1], R. Sussmann[2], and T. Warneke[1]

[1]Institute of Environmental Physics (IUP), University of Bremen FB1, Otto-Hahn-Allee 1, P.O. Box 33 04 40, 28334 Bremen, Germany
[2]Karlsruhe Institute of Technology, IMK-IFU, Garmisch-Partenkirchen, Germany

Correspondence to: J. Heymann (heymann@iup.physik.uni-bremen.de)

Received: 10 April 2012 – Published in Atmos. Meas. Tech. Discuss.: 13 June 2012
Revised: 6 September 2012 – Accepted: 11 September 2012 – Published: 9 October 2012

Abstract. Global observations of column-averaged dry air mole fractions of carbon dioxide (CO_2), denoted by XCO_2 , retrieved from SCIAMACHY on-board ENVISAT can provide important and missing global information on the distribution and magnitude of regional CO_2 surface fluxes. This application has challenging precision and accuracy requirements.

In a previous publication (Heymann et al., 2012), it has been shown by analysing seven years of SCIAMACHY WFM-DOAS XCO_2 (WFMDv2.1) that unaccounted thin cirrus clouds can result in significant errors.

In order to enhance the quality of the SCIAMACHY XCO_2 data product, we have developed a new version of the retrieval algorithm (WFMDv2.2), which is described in this manuscript. It is based on an improved cloud filtering and correction method using the 1.4 µm strong water vapour absorption and 0.76 µm O_2-A bands. The new algorithm has been used to generate a SCIAMACHY XCO_2 data set covering the years 2003–2009.

The new XCO_2 data set has been validated using ground-based observations from the Total Carbon Column Observing Network (TCCON). The validation shows a significant improvement of the new product (v2.2) in comparison to the previous product (v2.1). For example, the standard deviation of the difference to TCCON at Darwin, Australia, has been reduced from 4 ppm to 2 ppm. The monthly regional-scale scatter of the data (defined as the mean intra-monthly standard deviation of all quality filtered XCO_2 retrievals within a radius of 350 km around various locations) has also been reduced, typically by a factor of about 1.5. Overall, the validation of the new WFMDv2.2 XCO_2 data product can be summarised by a single measurement precision of 3.8 ppm, an estimated regional-scale (radius of 500 km) precision of monthly averages of 1.6 ppm and an estimated regional-scale relative accuracy of 0.8 ppm.

In addition to the comparison with the limited number of TCCON sites, we also present a comparison with NOAA's global CO_2 modelling and assimilation system CarbonTracker. This comparison also shows significant improvements especially over the Southern Hemisphere.

1 Introduction

Carbon dioxide (CO_2) is the most important anthropogenic greenhouse gas contributing to global warming. Reliable climate prediction requires an appropriate knowledge of its surface sources and sinks. Currently, this knowledge has large gaps (e.g. Stephens et al., 2007). Satellite observations of the column-averaged dry air mole fractions of CO_2 (denoted XCO_2) can close these gaps (Rayner and O'Brien, 2001; Houweling et al., 2004; Miller et al., 2007; Chevallier et al., 2007). This, however, requires a high accuracy and precision of the XCO_2 data product to constrain the surface fluxes of CO_2 significantly (Chevallier et al., 2007; Miller et al., 2007).

Measurements having near-surface sensitivity are needed for a sufficiently accurate inversion of regional CO_2 surface fluxes. At present, the only satellite instruments, which make such measurements are SCIAMACHY (SCanning Imaging Absorption spectroMeter of Atmospheric CHartographY)

on-board ENVISAT (ESA's ENVIronmental SATellite) (Burrows et al., 1995; Bovensmann et al., 1999; Buchwitz et al., 2007; Houweling et al., 2005; Bösch et al., 2006; Barkley et al., 2007; Schneising et al., 2012; Reuter et al., 2011) and TANSO (Thermal And Near infrared Sensor for carbon Observation) on-board GOSAT (Greenhouse gases Observing SATellite) (Yokota et al., 2004; Oshchepkov et al., 2008; Butz et al., 2009; Saitoh et al., 2009; Kuze et al., 2009; Yoshida Y. et al., 2011; Yoshida J. et al., 2011; Morino et al., 2011).

Several different retrieval algorithms have been developed (Buchwitz et al., 2006; Barkley et al., 2006a; Bösch et al., 2006; Schneising et al., 2012; Reuter et al., 2011) to obtain XCO_2 from SCIAMACHY measurements. The WFM-DOAS (Weighting Function Modified – Differential Optical Absorption Spectroscopy) retrieval algorithm (Buchwitz et al., 2000) is one of them. The version 2.1 of this algorithm has been used to generate the only available SCIAMACHY XCO_2 data set covering the years 2003–2009, which has been described in the peer-reviewed literature (Schneising et al., 2011, 2012). Heymann et al. (2012) compared the difference of these XCO_2 data and those from NOAA's (National Oceanic and Atmospheric Administration) modelling and assimilation system CarbonTracker (Peters et al., 2007) with global aerosol and cloud data. They found significant correlations with clouds in several regions especially over the Southern Hemisphere and concluded that the SCIAMACHY WFM-DOAS version 2.1 XCO_2 data product presumably suffers from the unaccounted scattering by thin clouds in those regions.

In order to reduce scattering related errors, retrieval algorithms have been developed which explicitly account for aerosols and clouds (Oshchepkov et al., 2008; Butz et al., 2009; Reuter et al., 2011; Yoshida Y. et al., 2011; O'Dell et al., 2012). Most of these algorithms are computationally very expensive. In contrast, WFM-DOAS is a computationally very fast algorithm because it uses a lookup table (LUT) approach that avoids time consuming online radiative transfer calculations. High processing speed is an important advantage especially for future satellites, such as CarbonSat (Carbon Monitoring Satellite) (Bovensmann et al., 2010) which will deliver orders of magnitude more observations than the current ones. On the other hand also demanding accuracy requirements have to be met.

The goal of this study is to determine to what extent the WFM-DOAS XCO_2 accuracy can be further improved by reducing scattering related errors. For this reason, we have developed an improved cloud filtering and correction method for SCIAMACHY WFM-DOAS XCO_2 retrievals that is based on a threshold technique for radiances from the saturated water vapour absorption band at 1.4 µm, which is described in this manuscript. With this method, an updated SCIAMACHY WFM-DOAS XCO_2 data set version 2.2 has been generated. In order to investigate if this method improves the satellite data, we intercompared SCIAMACHY WFM-DOAS XCO_2 version 2.2 with Fourier transform spectrometer (FTS) measurements at various TCCON sites and with recapitulated TCCON validation results of version 2.1 of Schneising et al. (2012). We also intercompared the satellite data with model output from NOAA's modelling and assimilation system CarbonTracker. In this study, the results of these intercomparisons are discussed.

This article is structured as follows: The next section gives a short overview of the satellite instrument SCIAMACHY. The WFM-DOAS retrieval algorithm is briefly introduced in Sect. 3. In Sect. 4 the new SCIAMACHY WFM-DOAS XCO_2 version 2.2 retrieval algorithm is presented followed by a description of the used data sets for the comparison with the satellite data in Sect. 5. A discussion of the intercomparison results with the measurements from TCCON FTS sites is described in Sect. 6. The results of the intercomparison with CarbonTracker are discussed in Sect. 7. Finally, conclusions are given in Sect. 8.

2 SCIAMACHY

SCIAMACHY (SCanning Imaging Absorption spectroMeter for Atmospheric CHartographY) is a grating spectrometer and a national contribution to the atmospheric chemistry payload of ESA's (European Space Agency) ENVISAT (ENVIromental SATellite) (Burrows et al., 1995; Bovensmann et al., 1999). The satellite was launched in March 2002 into a sun-synchronous daytime (descending) orbit with an equator crossing time of 10:00 a.m. SCIAMACHY continuously measures reflected, backscattered and transmitted solar radiation in six channels covering the spectral region 214–1750 nm and in two additional channels covering the 1940–2040 nm and the 2265–2380 nm regions. The spectral resolution ranges from 0.2 to 1.4 nm. In addition to the eight main channels, seven polarisation measurement devices (PMD) measure upwelling broad band radiation polarised with respect to the instrumental plane with higher spatial resolution.

The satellite instrument performs measurements in four different observation modes: solar and lunar occultation and limb and nadir. For this study nadir observations from channel 4 (605–805 nm; for O_2), channel 6 (1000–1750 nm; for CO_2 and water vapour) and PMD 1 (320–380 nm) are used. The integration time of the instrument in the used spectral regions of channels 4 and 6 is typically 0.25 s and provides a typical spatial resolution of 60 km across track by 30 km along track. A total swath width of 960 km is achieved by scanning across-track $\pm 32^\circ$ relative to direct nadir viewing.

3 SCIAMACHY WFM-DOAS v2.1

The WFM-DOAS retrieval algorithm is described in detail in Schneising et al. (2011). Here, we give a short overview of the algorithm.

The WFM-DOAS retrieval algorithm was developed to retrieve accurate vertical columns of atmospheric gases like O_2, CO_2, CH_4, etc. from SCIAMACHY measurements. The algorithm utilises a least-squares method, which scales preselected atmospheric vertical profiles. For the retrieval of the CO_2 and O_2 column, sun-normalised radiances from spectra covering the O_2-A absorption band at 755–775 nm and CO_2 absorption lines between 1558–1594 nm are used. The logarithm of a linearised radiative transfer model is fitted to the logarithm of the measured radiances. A fast lookup table approach is used to avoid computationally expensive radiative transfer simulations. The fit parameters yield the CO_2 and O_2 columns. The simultaneously retrieved O_2 column is used as a light path proxy for CO_2 and is needed to convert CO_2 columns (molec cm^{-2}) into XCO_2 (ppm).

Aerosols are considered by using a constant aerosol vertical profile for the radiative transfer simulations. In addition, the aerosol variability is considered (i) by using O_2 as a light path proxy, (ii) by the low-order DOAS polynomial that makes the retrieval insensitive to spectrally broadband radiance modifications, and (iii) by using the SCIAMACHY Absorbing Aerosol Index (AAI) data product (Tilstra et al., 2007) to identify and filter scenes contaminated with high loads of aerosols.

The WFM-DOAS algorithm also includes a cloud detection algorithm, which is based on a threshold technique for the normalised and solar zenith angle corrected PMD 1 signal and the deviation of the retrieved O_2 column from the assumed a priori O_2 column. If the cloud detection algorithm detects a cloud, the corresponding ground pixel will be flagged as cloudy. For the identification of successful retrievals a binary quality flag (good/bad) is used, which is part of the XCO_2 data product.

Heymann et al. (2012) found a scan-angle dependent bias in the SCIAMACHY WFMDv2.1 XCO_2 data set. This bias was corrected using an empirical correction method. A comparison of the scan-angle bias corrected and uncorrected SCIAMACHY XCO_2 data set with CarbonTracker showed better agreement of the scan-angle bias corrected data product. In this study, we use the scan-angle bias corrected and quality filtered SCIAMACHY WFM-DOAS v2.1 level 2 data product for the period 2003–2009.

4 New SCIAMACHY WFM-DOAS v2.2 algorithm

The improved SCIAMACHY WFM-DOAS v2.2 XCO_2 algorithm is described in the following.

4.1 Improved cloud filtering and correction method

The cloud filter as implemented in the WFMDv2.1 XCO_2 algorithm is based on two approaches: (i) a filtering method based on sub-pixel information of SCIAMACHY's polarisation measurement device (PMD) 1 and (ii) a threshold technique for the ratio of the retrieved to the reference O_2 column. Both approaches are described in detail, e.g. in Heymann et al. (2012).

For WFMDv2.2 these filtering approaches are extended by (i) a threshold technique based on the radiance from the saturated water vapour absorption band at 1.4 µm, (ii) by using stricter thresholds for the ratio of the retrieved O_2 column to the reference column, and (iii) a restriction to surface elevations of less than 4 km. In addition, a correction method of XCO_2 based on the statistics of the O_2 column ratio is applied. Overall, the new filtering approach identifies about 25 % more observations which are contaminated with clouds (from a total amount of about 5.65×10^6 cloud-free ground pixels for WFMDv2.1 for the years 2003–2009 to about 4.24×10^6 for WFMDv2.2).

The restriction of the surface elevation is made because of LUT limitations. The other filtering methods are described within the next sections.

4.1.1 Use of the saturated water vapour absorption band at 1.4 µm

In this section, the threshold technique, developed in this study and based on the saturated water vapour absorption band at 1.4 µm, is described. We use this band to detect and remove thin cirrus clouds. Gao et al. (1993) showed that the saturated water vapour band is sensitive to high thin cirrus clouds and can be used for cirrus cloud detection. This is because in the clear sky case, the amount of radiation measured from space in nadir mode is very small as essentially all photons are absorbed by tropospheric water vapour. When a cirrus cloud is located above almost all of the atmospheric water vapour is present, a significant amount of radiation can be backscattered and measured. Our implementation of this detection method is as follows.

We use sun-normalised radiance (intensity) spectrally averaged between 1.395–1.41 µm measured by 20 detector pixels of SCIAMACHY channel 6. We spectrally average the intensity to reduce the measurement error to about 0.1 %. Within this interval, the integration time of the detector is the same as in the O_2 and CO_2 fit windows used by WFM-DOAS. If the measured intensity (I_{meas}) of a ground pixel is three times larger than a reference intensity (I_0, corresponding to the clear sky case), the ground pixel will be flagged as cloudy. The left panel of Fig. 1 shows the deviation of the measured intensity from a reference intensity for SCIAMACHY WFM-DOAS v2.1. The cloud filtering threshold is shown in the right panel (the deviation has to be larger than $P_{\mathrm{H_2O}} = 2.0$, shown by the red line), which represents a compromise between cloud filtering and the loss of too much data. Figure 2 shows the used reference intensity as a function of the water vapour vertical column amount (H_2O^{VCA}) and the number of occurrences for WFMDv2.1 between 2003 and 2009. To ensure that we only use cloud-free measurements for the statistical assessment

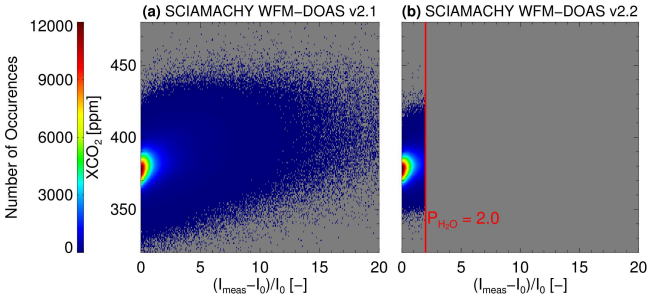

Fig. 1. Deviations between measured sun-normalised radiances (intensity) spectrally averaged between 1.395–1.41 µm (I_{meas}) and the reference intensities (I_0) for SCIAMACHY WFM-DOAS version 2.1 **(a)** and 2.2 **(b)** using all data of the years 2003 – 2009. **(a)** A 2-D histogram of XCO_2 as a function of the deviation between I_{meas} and I_0. **(b)** as in **(a)** but for WFMDv2.2. The red line indicates the cloud filtering threshold ($P_{H_2O} = 2.0$).

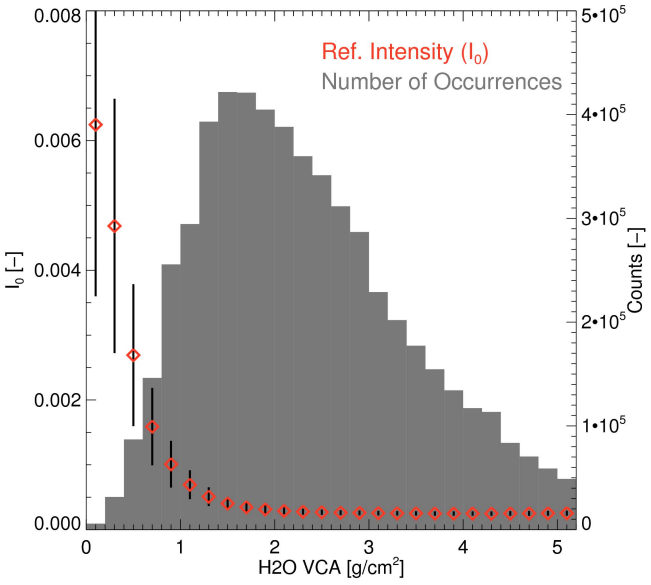

Fig. 2. Analysis of 1.4 µm (1390 nm–1410 nm) radiances as measured by SCIAMACHY for the years 2003–2009. The red diamonds show the reference intensity (I_0) as a function of the water vapour vertical column amount (H_2O VCA). The reference intensity is defined as the mean of the 40 % lowest values of the (sun-normalised) radiances (corresponding to scenes with no clouds or very small effective cloud cover). The black vertical lines are the corresponding standard deviations. The grey histogram shows the number of occurrences as a function of the water vapour vertical column amount.

of the reference intensity, we have averaged the 40 % lowest intensities within each H_2O^{VCA} interval. As can be seen, the reference intensity is nearly constant if the H_2O^{VCA} is larger than 1 g cm^{-2}. With decreasing H_2O^{VCA}, the reference intensity increases and its standard deviation as well. However, only a small fraction of the retrieved H_2O^{VCA} is lower than 1 g cm^{-2} and the relaxed filtering threshold prevents too much clear sky data from being flagged as cloudy. The distribution of the WFMDv2.1 data shows a maximum for H_2O^{VCA} between 1.4 and 1.6 g cm^{-2}, which is similar to the 1.42 g cm^{-2} of the US standard atmosphere.

The H_2O^{VCA} used in this study is computed from the WFM-DOAS simultaneously retrieved water vapour column in the CO_2 fit window and is given in the Level 2 (L2) data product of WFMDv2.1. Figure 3 shows a comparison with water vapour vertical column amounts obtained from ECMWF. A global offset (d) of -0.31 g cm^{-2}, a standard deviation of the difference between the data sets (s) of 0.53 g cm^{-2}, and a correlation coefficient of 0.89 show reasonable agreements between the two data sets. This indicates that reasonable cloud-free H_2O columns can be retrieved from the CO_2 fit window of WFM-DOAS at 1.6 µm and can be used for the filtering approach.

A more quantitative estimation of the sensitivity of this filtering method has been performed by using radiative transfer simulations. Figure 4 shows deviations of simulated intensities to simulated clear sky intensities for various cloud scenarios with different water vapour vertical column amounts. The scenario of the radiative transfer simulations has been defined as follows: only direct nadir conditions (viewing zenith angle of 0°) are considered. In order to simulate cirrus clouds, an ice cloud with fractal particles based on a tetrahedron with an edge length of 50 µm, with a cloud top height (CTH) of 10 km and a geometrical thickness of 0.5 km is used. The used aerosol profile (default aerosol profile) is based on a realistic aerosol scenario (see the OPAC background scenario) described by Schneising et al. (2008). For Fig. 4 an albedo of 0.1 and a solar zenith angle (SZA) of 40° has been used. The intersections with the filtering threshold $P_{H_2O} = 2.0$ represent the minimum detectable cloud optical depth (COD) of a cloud which can be detected (note that homogeneous cloud cover is assumed). For increasing water vapour vertical column amounts, the minimum detectable COD decreases and the sensitivity increases but only slightly for column amounts larger than 1 g cm^{-2}. The filtering approach is insensitive to clouds if only a very small amount of water vapour is present in the atmospheric column.

Table 1 summarises the results of all simulation scenarios. For the case of water vapour vertical column amounts being larger than 1.14 g cm^{-2}, the filter becomes insensitive to SZA, CTH (assuming CTH > 4 km) and albedo. For column amounts below 1.14 g cm^{-2} the sensitivity decreases and the filter is more dependent on geometry and surface albedo. The filter is insensitive for low thin clouds (CTH < 4 km). In this case, the absorption band becomes already saturated above the cloud if enough water vapour is in the atmospheric column. This can also effect the sensitivity for high clouds but only for large H_2O^{VCA}.

The saturated water vapour absorption band based cloud filter is sensitive to thin (COD > 0.05) and high (CTH > 4 km) clouds if the observed atmospheric column contains

Table 1. Minimum detectable cloud optical depth (COD) for the cloud detection algorithm based on a threshold method for the radiance of the saturated water vapour absorption band at 1.4 µm for various simulation scenarios as defined by solar zenith angle (SZA), surface albedo (ALB), cloud top height (CTH) and water vapour vertical column amount. The default aerosol scenario and a cloud geometrical thickness of 0.5 km have been used for all scenarios. ∞ means that even clouds with large COD are not detected.

Minimum detectable COD										
SZA [°]	ALB [–]	CTH [km]	Water vapour vertical column amount [g cm^{-2}]									
			0.00	0.14	0.29	0.57	0.86	1.14	1.43	2.86	4.29	7.15
20	0.1	10	4.76	0.98	0.58	0.25	0.13	0.08	0.05	0.03	0.03	0.03
40	0.1	10	3.68	0.72	0.40	0.16	0.08	0.05	0.03	0.02	0.02	0.02
60	0.1	10	2.40	0.34	0.16	0.06	0.03	0.02	0.01	0.01	0.01	0.01
40	0.3	10	23.74	2.04	1.04	0.41	0.19	0.10	0.06	0.02	0.02	0.02
40	0.6	10	∞	4.76	2.08	0.74	0.33	0.16	0.09	0.02	0.02	0.02
40	0.1	16	3.68	0.70	0.39	0.15	0.07	0.04	0.03	0.02	0.02	0.01
40	0.1	13	3.68	0.71	0.39	0.15	0.08	0.04	0.03	0.02	0.02	0.02
40	0.1	7	3.68	0.81	0.48	0.21	0.11	0.07	0.05	0.04	0.04	0.05
40	0.1	4	3.68	1.17	0.80	0.44	0.27	0.19	0.16	0.19	0.31	0.73

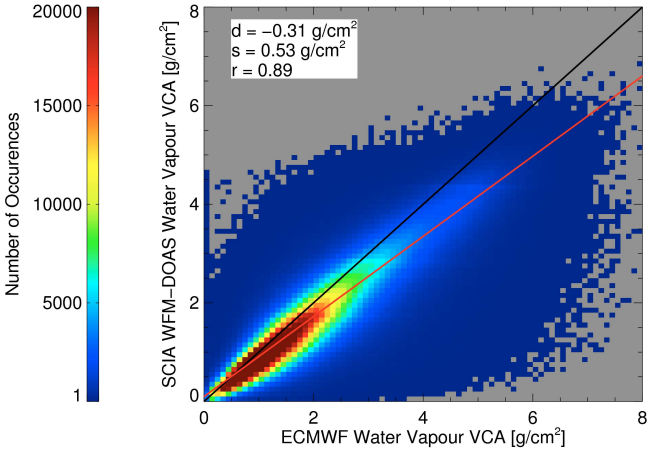

Fig. 3. Comparison of seven years (2003–2009) of SCIAMACHY WFM-DOAS and ECMWF water vapour vertical column amount (VCA). The SCIAMACHY WFM-DOAS water vapour VCA is computed from the water vapour column retrieved in the CO_2 fitting window (1558–1594 nm) as a by-product of the WFM-DOAS CO_2 column retrieval. The red line shows a linear fit. Also shown in the top left inlet: the mean difference to ECMWF water vapour VCA (d), the standard deviation of the differences (s) and the correlation coefficient (r).

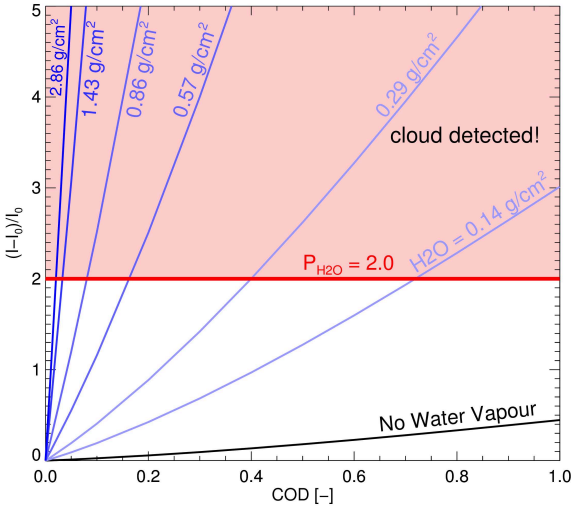

Fig. 4. The cloud detection threshold (red horizontal line) based on strong water vapour absorption lines covering the spectral region 1395–1410 nm compared to results obtained from radiative transfer simulations. Deviations of simulated intensities (I) for various cloud scenarios to the reference intensities (I_0) simulated without cloud are shown as a function of cloud optical depth (COD) and different water vapour column amounts (H_2O [g cm^{-2}]) . The simulations are valid for a solar zenith angle of 40°, a surface albedo of 0.1, the default aerosol scenario, a cloud top height of 10 km and a cloud geometrical thickness of 0.5 km. The red line indicates the cloud detection threshold $P_{H_2O} = 2.0$.

enough water vapour ($H_2O^{VCA} > 1.14\,g\,cm^{-2}$). The WFM-DOAS XCO_2 data set suffers from thin and high clouds in the tropics especially in the Southern Hemisphere, as shown by Heymann et al. (2012). For this reason, this filter approach is an appropriate extension to the existing cloud filtering criteria.

4.1.2 Use of O_2 column ratios

As described by Schneising et al. (2011) for WFMDv2.1, ground pixels with deviations of the retrieved O_2 column to the reference O_2 column (O_2 ratio) smaller than 0.9 are identified and flagged as cloudy. The reference O_2 column

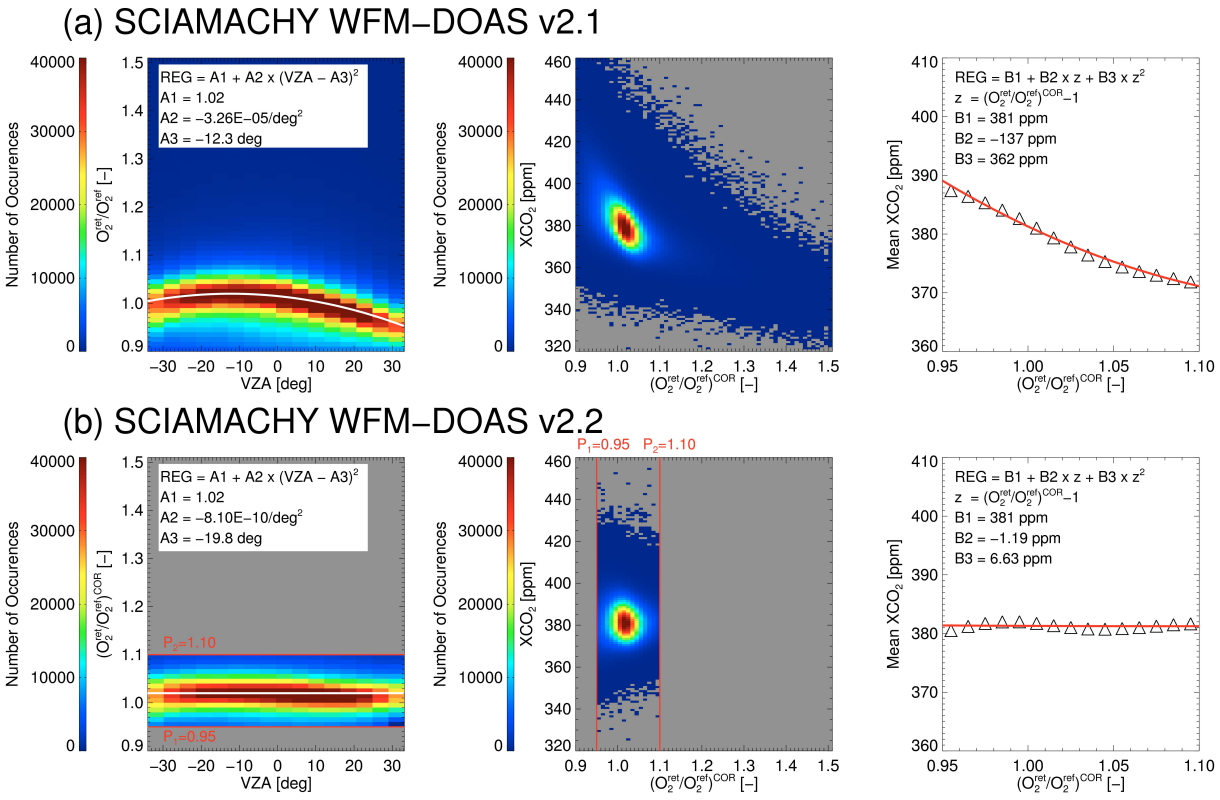

Fig. 5. Comparison of the O_2-column ratio (O_2^{ret}/O_2^{ref}) for SCIAMACHY WFM-DOAS version 2.1 **(a)** and 2.2 **(b)** using all data from the years 2003–2009. **(a)** The left panel shows a 2-D-histogram of the O_2 ratio as a function of the viewing zenith angle (VZA). The white curve is a quadratic fit. The middle panel shows a 2-D-histogram of XCO_2 as a function of the scan-angle bias corrected O_2 ratio. The right panel shows XCO_2 averaged over scan-angle bias corrected O_2 ratio intervals. The red curve is a polynomial fit. **(b)** as in **(a)** but for WFM-DOAS version 2.2. The red lines in the left and middle panel indicate the new O_2 ratio thresholds ($P_1 = 0.95$ and $P_2 = 1.1$).

is determined from the US standard atmosphere O_2 column by accounting for the surface elevation variations in order to obtain the same O_2 ratio as used by Schneising et al. (2011). Heymann et al. (2012) showed that clouds with eCOD (effective cloud optical depth defined as cloud fractional coverage times cloud optical depth) less than 0.1 may remain undetected. These undetected clouds can cause systematic errors, which are significant for the CO_2 surface flux inversion application. For this reason, we have also investigated to what extent a more restrictive O_2 ratio threshold can improve the quality of the XCO_2 data product.

A geometrical viewing geometry correction has been implemented for the O_2 and CO_2 column in WFM-DOAS in order to correct for a scan-angle dependent air-mass factor (Buchwitz and Burrows, 2004). For this reason, the O_2 vertical column ratio should be independent of the viewing geometry. However, we found that the O_2 ratio exhibits a scan-angle dependent bias. In order to improve the geometrical correction, we correct for this bias using an empirical correction. A quadratic function depending on the (signed) viewing zenith angle (VZA) (as defined by Heymann et al., 2012) was fitted to the O_2 ratio and used for the correction:

$$(O_2^{ret}/O_2^{ref})^{cor} = O_2^{ret}/O_2^{ref} + A_2 \cdot (VZA - A_3)^2 \quad (1)$$

O_2^{ret} corresponds to the retrieved and O_2^{ref} to the reference O_2 column. A_2 is $3.26 \times 10^{-5} \frac{1}{(°)^2}$ and A_3 is $-12.3°$. These values are adapted from the fit shown in the top left panel of Fig. 5. This figure shows the scan-angle dependency before the scan-angle bias correction of the O_2 ratio of WFMDv2.1 in the top left panel and after the scan-angle bias correction for WFMDv2.2 in the bottom left panel.

We use the scan-angle bias corrected O_2 ratio for cloud filtering in the following way: If the O_2 ratio of a ground pixel exceeds 1.1 or is smaller than 0.95, the ground pixel is flagged as cloudy. O_2 ratios smaller than 1 indicate a light path shortening (e.g. due to cloud shielding), whereas O_2 ratios larger than 1 indicate a light path lengthening (e.g. due to multiple scattering). For this reason, we increase the lower threshold of 0.9 of WFMDv2.1 to 0.95 and we added the upper threshold of 1.1.

We have performed various simulations to study the relation of XCO_2 and the O_2 ratio in the presence of thin clouds and aerosols. We found a strong and nearly linear dependency of XCO_2 on the O_2 ratio for simulation scenarios (same default scenario as in Sect. 4.1.1) with different

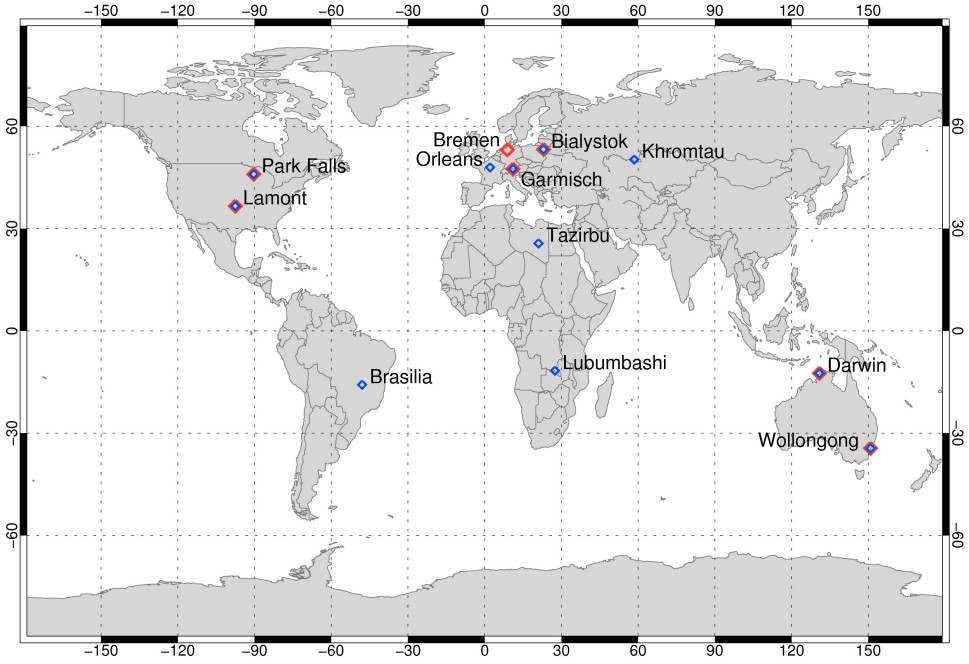

Fig. 6. Locations analysed in this study. The red diamonds show the locations used for the comparison of WFMD versions 2.1 and 2.2 with FTS measurements. The blue diamonds show the locations used for the determination of the monthly regional-scale scatter of the data in Sect. 4.2.

Table 2. Scatter of the WFMDv2.1 and v2.2 XCO_2 data products at several locations and overall (MEAN).

Monthly regional-scale scatter of the data							
Location	Country	Lat [°]	Lon [°]	WFMDv2.1		WFMDv2.2	
				abs [ppm]	rel [%]	abs [ppm]	rel [%]
Bialystok	Poland	53.2	23.0	6.09	1.59	4.61	1.21
Khromtau	Kazakhstan	50.3	58.5	9.23	2.43	4.68	1.23
Orleans	France	48.0	2.1	6.28	1.64	4.48	1.17
Garmisch	Germany	47.5	11.1	8.09	2.14	5.56	1.46
Park Falls	USA	46.0	−90.3	7.65	2.01	5.29	1.39
Lamont	USA	36.6	−97.5	7.56	1.99	4.01	1.05
Tazirbu	Libya	25.7	21.4	4.95	1.30	3.48	0.91
Lubumbashi	Congo	−11.7	27.5	9.09	2.39	4.68	1.23
Darwin	Australia	−12.4	130.9	7.20	1.88	3.80	1.00
Brasilia	Brazil	−15.8	−47.9	8.26	2.16	4.52	1.19
Wollongong	Australia	−34.4	150.9	7.17	1.89	4.52	1.19
MEAN				7.42 ± 1.29	1.95 ± 0.34	4.51 ± 0.60	1.18 ± 0.16

SZA, surface albedos and optical depths. The reason for this dependency is different light paths in the retrieval of the O_2 and CO_2 columns used spectral regions due to scattering by aerosols and thin clouds. Therefore, we have investigated if a reference O_2 column obtained from ECMWF (European Centre for Medium-Range Weather Forecasts) surface pressure and used for the normalisation of the CO_2 column improves the quality of the XCO_2 data product. However, we find large regional patterns, a much larger intra-monthly scatter, larger seasonal cycle amplitudes and significant lower yearly increases over the Northern and Southern Hemisphere. Overall, we find that using a reference O_2 column reduces the quality of the SCIAMACHY WFM-DOAS XCO_2 data product. Therefore, we keep on using the retrieved O_2 column for the normalisation of the CO_2 column and correct for the bias between XCO_2 and the O_2 ratio using a statistical method. We assume that other features responsible for the O_2 ratio dependent bias in XCO_2 rather

than scattering by aerosols and thin clouds can be neglected. We use a polynomial fitted to averaged XCO_2 and O_2 ratios:

$$XCO_2^c = XCO_2 + B_1 + B_2 \cdot z + B_3 \cdot z^2 \quad (2)$$
$$z = ((O_2^{ret}/O_2^{ref})^{cor} - 1).$$

Here B_1 is -0.8 ppm and accounts for a global offset. B_2 is 137 ppm and B_3 is -362 ppm. The fit parameters shown in Fig. 5 top-right are used for this correction. The bottom-right and mid-panels in this figure show the resulting dependency of XCO_2 on the O_2 ratio after applying the improved filter method. As can be seen, the stricter O_2 ratio thresholds remove unrealistic high and low values of XCO_2 and the remaining O_2 ratio dependent bias in XCO_2 is very small.

4.2 Single measurement precision

Heymann et al. (2012) determined the monthly regional-scale scatter of the SCIAMACHY WFMDv2.1 XCO_2 data product of about 7.42 ± 1.29 ppm. We have used the same method to determine this value for the new version 2.2 data product.

The scatter is derived as follows: we compute the standard deviation of all XCO_2 measurements within a radius of 350 km around several locations for each month. The locations used for this assessment are shown in Fig. 6 and their latitudes and longitudes are listed in Table 2. We have selected the same locations as used by Heymann et al. (2012). For these locations sufficient XCO_2 data are available and they are distributed over all continents covered by the data. The mean of the monthly standard deviations is derived for all locations. The overall value of the scatter is the mean of the scatter of all locations. This value is not only determined by instrumental and retrieval noise. Atmospheric XCO_2 variability and systematic errors can also affect this value (note that the seasonal cycle is filtered out by using the standard deviations of the monthly data). However, the computed monthly regional-scale scatter of the data can be regarded as an upper limit of the single measurement precision.

The standard deviations of WFMDv2.1 and WFMDv2.2 XCO_2 are listed in Table 2. As can be seen, the standard deviation is smaller for version 2.2. The monthly regional-scale scatter is reduced to 4.51 ± 0.60 ppm for WFMDv2.2 compared to 7.42 ± 1.29 ppm for WFMDv2.1.

In addition, we estimated the single measurement precision using the same approach as used in the publication of Schneising et al. (2011). They estimated the precision by averaging daily standard deviations of the retrieved XCO_2 for 8 locations distributed around the globe. This estimation shows a reduction of the single measurement precision from 5.4 ppm (1.4 %) of WFMDv2.1 to 3.8 ppm (1 %) of WFMDv2.2.

5 Data sets used for comparison

In this section, the data sets used for the comparison with the new SCIAMACHY WFM-DOAS XCO_2 version 2.2 as well as with the previous version 2.1 data product are briefly described.

5.1 TCCON

We use the independent measurements from the ground-based Fourier transform spectrometers (FTS) of TCCON (Total Carbon Column Observing Network) for the validation of the SCIAMACHY WFMDv2.2 XCO_2 data product. TCCON is a global network of ground-based FTS instruments and provides measurements of CO_2 and other greenhouse gases (Wunch et al., 2011). The FTS measurements are the most important validation source for measurements from satellite instruments like SCIAMACHY and GOSAT and future satellite missions like OCO-2 (Crisp et al., 2004; Bösch et al., 2011) and CarbonSat (Bovensmann et al., 2010). A stable and robust commercial high-resolution FTS, the Bruker IFS 125/HR, is used as standard instrument and common data processing and analysis software is utilised to determine XCO_2 with a high accuracy of approximately 0.2 % (Wunch et al., 2011).

We obtained the FTS data from the TCCON website (http://www.tccon.caltech.edu) and use monthly means in this study.

5.2 CarbonTracker

For a global comparison of the SCIAMACHY WFM-DOAS v2.1 and v2.2 XCO_2 , we use NOAA's global CO_2 modelling and assimilation system CarbonTracker. CarbonTracker has been developed to estimate the global atmospheric CO_2 distribution and the CO_2 surface fluxes (Peters et al., 2007). CarbonTracker assimilates precise and accurate measurements of NOAA's greenhouse gas air sampling network. Version 2010 of CarbonTracker for the years 2003–2009 has been downloaded from http://carbontracker.noaa.gov. In order to obtain daily CarbonTracker XCO_2 , the CarbonTracker CO_2 vertical profiles have been vertically integrated after applying the averaging kernels of the SCIAMACHY WFM-DOAS XCO_2 retrieval algorithm. This daily CarbonTracker XCO_2 data set has been regridded on a latitude/longitude grid and sampled like the SCIAMACHY measurements.

6 Validation with TCCON FTS measurements

In order to investigate whether the filtering and correction method improves the quality of the SCIAMACHY XCO_2 data product, we have compared the new WFMDv2.2 data set with the independent TCCON FTS measurements and intercompared the results with validation results for WFMDv2.1

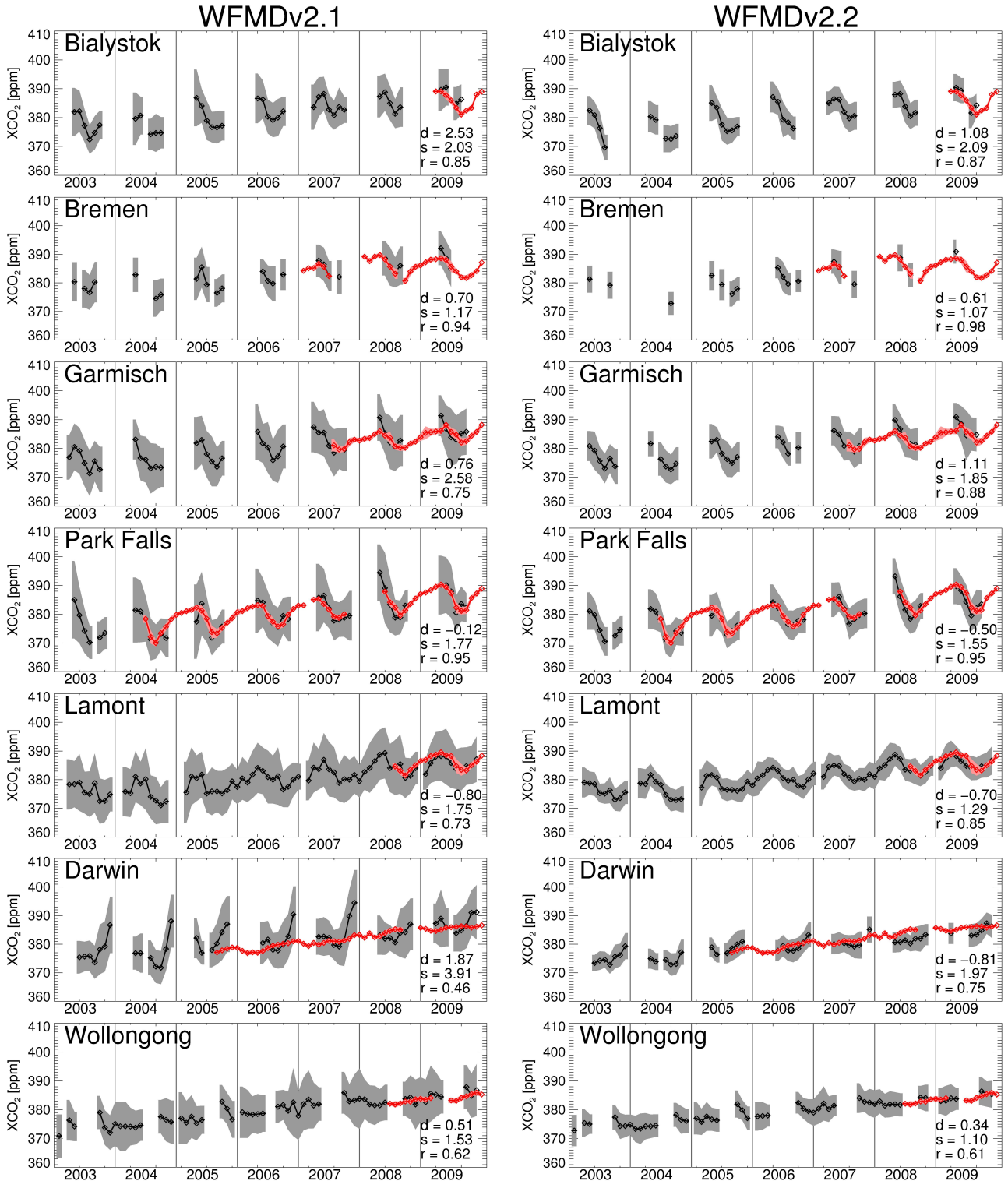

Fig. 7. Comparison of monthly averaged SCIAMACHY WFM-DOAS version 2.1 (left) and 2.2 (right) XCO_2 (black) with Fourier transform spectroscopy (FTS) measurements (red) at various TCCON sites for the years 2003–2009. The monthly standard deviations are represented by the shaded areas (grey: WFMD; light red: TCCON). In addition, the mean difference (d [ppm]), the standard deviation of the difference (s [ppm]) and the correlation (r [-]) between the satellite and ground based data are shown (see also Table 3).

Table 3. Results of the comparison of WFMDv2.1 and v2.2 XCO_2 data with ground based FTS measurements at various TCCON sites. The comparison is based on monthly data. Shown are the number of months used for the comparison (n), the mean difference to FTS (d), the standard deviation of the difference (s) and the correlation (r). In addition, the following quantities are given in the bottom row (MEAN): the averaged mean difference (global offset), the standard deviation of the mean differences (relative regional-scale accuracy), the mean standard deviation of the differences (monthly regional-scale precision) and the mean correlation.

TCCON Site	Lat [°]	Lon [°]	WFMDv2.1				WFMDv2.2			
			n [–]	d [ppm]	s [ppm]	r [–]	n [–]	d [ppm]	s [ppm]	r [–]
Bialystok	53.2	23.0	4	2.53	2.03	0.85	4	1.08	2.09	0.87
Bremen	53.1	8.8	9	0.70	1.17	0.94	5	0.61	1.07	0.98
Garmisch	47.5	11.1	14	0.76	2.58	0.75	13	1.11	1.85	0.88
Park Falls	46.0	−90.3	35	−0.12	1.77	0.95	35	−0.50	1.55	0.95
Lamont	36.6	−97.5	16	−0.80	1.75	0.73	16	−0.70	1.29	0.85
Darwin	−12.4	130.9	31	1.87	3.91	0.46	28	−0.81	1.97	0.75
Wollongong	−34.4	150.9	9	0.51	1.53	0.62	7	0.34	1.10	0.61
MEAN			–	0.78 ± 1.13	2.11	0.76	–	0.16 ± 0.83	1.56	0.84

(Schneising et al., 2012). In this section, the result of this intercomparison are discussed.

6.1 Validation method

The validation of the WFMDv2.2 XCO_2 is performed in the same way as described in the publication of Schneising et al. (2012) for WFMDv2.1. This implies that monthly means for the time period 2003–2009 computed using a sufficiently large number of measurements within a radius of 500 km around the analysed TCCON sites (Bialystok, Bremen, Garmisch, Park Falls, Lamont, Darwin and Wollongong) are used. The locations of the TCCON sites are shown in Fig. 6 and the corresponding latitudes and longitudes are listed in Table 3.

From the monthly time series of the satellite and FTS data statistical quantities are determined for every FTS site: the regional bias (d) (mean difference to FTS measurements), the mean standard deviation of the difference (s) and the linear correlation coefficient (r) with the FTS measurements. From these values we determine the offset, the monthly regional-scale precision (the mean standard deviation of the difference to FTS), the mean correlation and the regional-scale relative accuracy (the standard deviation of the station-to-station biases).

The FTS and the satellite measurements provide information on the retrieved CO_2 column from different heights because of differing height sensitivities, as characterised by their averaging kernels. In order to compare these measurements, we use the comparison approach described by Rodgers (2000). The retrieved satellite and FTS CO_2 columns have been adjusted to a common a priori profile. For this study, we use the same adjustment method as described by Reuter et al. (2011) and Schneising et al. (2012).

6.2 Validation results

The results of the comparison of the WFMDv2.1 and WFMDv2.2 XCO_2 data product with the TCCON FTS measurements are shown in Fig. 7 and summarised in Table 3.

The comparison of WFMDv2.1 XCO_2 with the FTS measurements for Darwin, Australia, shows a large monthly scatter of the data (7.2 ppm) and large differences to the FTS (3.9 ppm). This is improved for the new WFMDv2.2 XCO_2 data product. The scatter is reduced to 3.8 ppm. The large deviation to the FTS is improved by nearly a factor of 2 (from 3.9 ppm to 2.0 ppm). The improvement is also shown by a higher correlation (0.75) between the satellite and the FTS data.

Overall, the comparison of WFMDv2.2 XCO_2 with FTS shows much better agreement than for WFMDv2.1. The monthly regional-scale precision has been improved from 2.1 ppm for WFMDv2.1 to 1.6 ppm for WFMDv2.2. The regional-scale relative accuracy has been improved from 1.1 ppm to 0.8 ppm and the mean correlation has been improved from 0.76 to 0.84.

These results show that the improved cloud filtering and correction method for WFMDv2.2 significantly improves the quality of the XCO_2 data product.

7 Comparison with CarbonTracker XCO_2

In addition to the comparison with the limited number of TCCON sites, we have also performed a comparison of WFMDv2.2 XCO_2 with global model results using NOAA's CarbonTracker.

Figure 8 shows three monthly averaged (April to June and July to September) global maps of WFMDv2.2 and CarbonTracker XCO_2 for the years 2003 and 2009. We have gridded the data on a $0.5° \times 0.5°$ latitude/longitude grid. Furthermore, we have smoothed the data by using a 2D-Hann window with

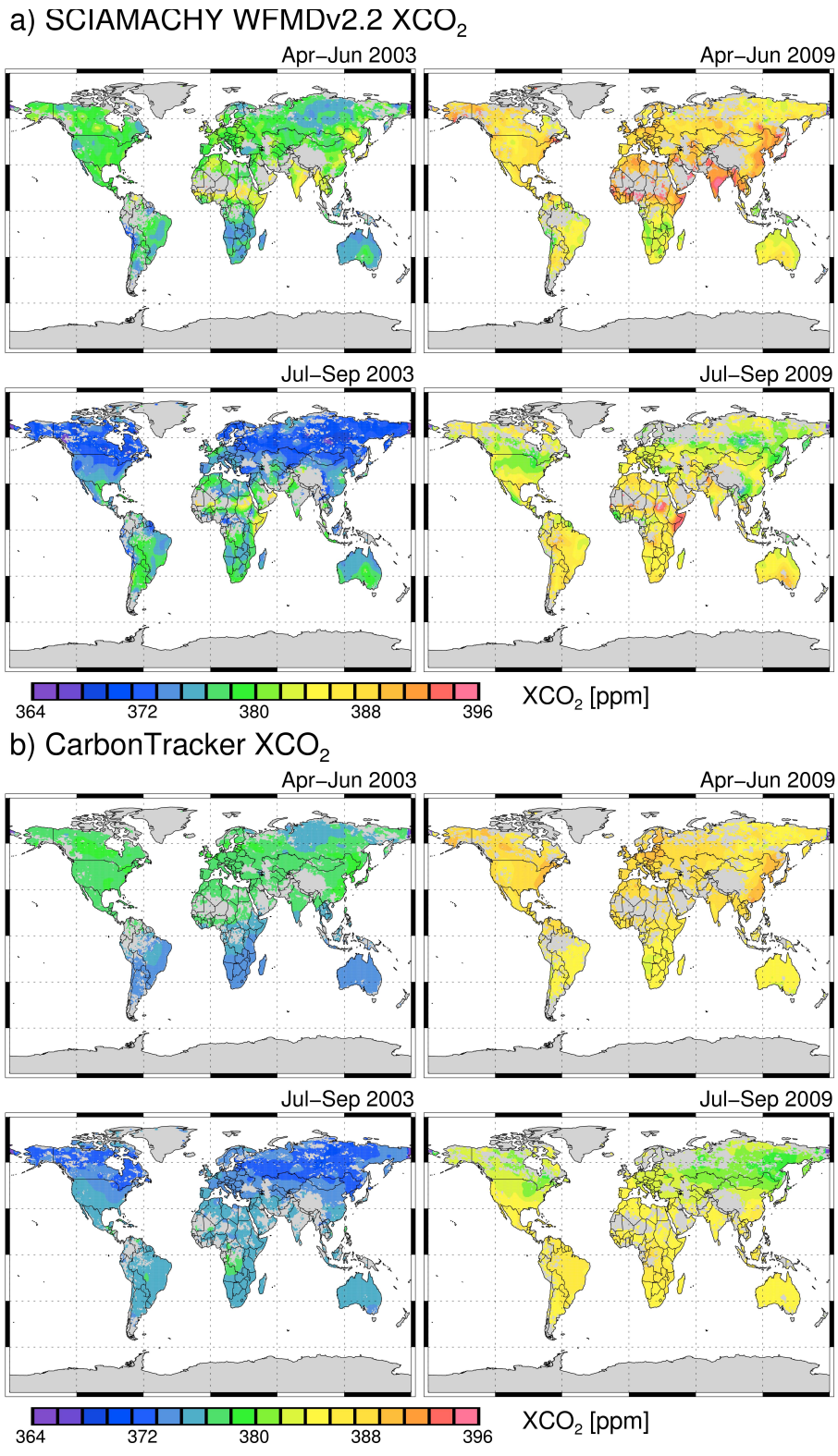

Fig. 8. Comparison between global SCIAMACHY and CarbonTracker XCO_2 . **(a)** Global SCIAMACHY WFMDv2.2 XCO_2 maps for the time periods April–June and July–September in 2003 and 2009. The data have been gridded on a $0.5° \times 0.5°$ latitude/longitude grid and smoothed by using a 2-D-Hann window with a width of 20×20 ($10° \times 10°$). **(b)** as in **(a)** but for CarbonTracker XCO_2 sampled as the SCIAMACHY measurements.

a width of 20×20 ($10° \times 10°$) because some grid boxes do not have sufficient data to remove the statistical error. The SCIAMACHY XCO_2 maps also show that with the much stricter cloud filtering and correction method good coverage of most land surfaces is achieved. There are however some gaps, e.g. Sahara and Himalaya, similar to WFMDv2.1. The maps of the SCIAMACHY and CarbonTracker XCO_2 also show the northern hemispherical terrestrial vegetation induced carbon uptake in summer as shown by higher XCO_2 values in April–June compared to lower XCO_2 values in July–September in 2003 and 2009. In addition, the increase of the global CO_2 concentration is seen by the higher XCO_2 in 2009 compared to 2003. Both data sets show reasonable agreement. There are, however, also significant differences, e.g. over India and the Horn of Africa, which needs further investigation.

For a more quantitative investigation, we compared WFMDv2.2 with CarbonTracker XCO_2 using hemispherical monthly means between 2003 and 2009. In order to investigate if the improved cloud filtering and correction method reduces the difference to CarbonTracker, we compare with WFM-DOAS v2.1 XCO_2 . However, it has to be noted that CarbonTracker is affected by errors of its own like, e.g. incorrect accounting for the vertical transport and the ageing of air and uncertainties in the biosphere fluxes (Basu et al., 2011).

Important parameters for the comparison are determined in the following way: the annual increase is determined by smoothing the time series with a twelve-month boxcar function and computing the mean from the derivative of the smoothed time series. The seasonal cycle amplitude is determined from a detrended time series between 2004 and 2008 by averaging the yearly difference of maximum and minimum XCO_2 . The error of the increase and the amplitude is estimated by a bootstrap method (see Schneising et al., 2011). The correlation with CarbonTracker and the standard deviation of the difference to CarbonTracker has been determined. In addition, the detrended correlation coefficient (r) to CarbonTracker is computed from the detrended time series of WFMDv2.1 and WFMDv2.2 and is an indicator for (phase) shifts between the time series.

Figure 9 shows the result of this comparison. As can be seen, the scatter is reduced from 10.2 ppm for WFMDv2.1 to 5.8 ppm for WFMDv2.2 for the Northern Hemisphere and from 9.2 ppm to 4.6 ppm for the Southern Hemisphere. The correlation with CarbonTracker is for both WFM-DOAS versions and for both hemispheres nearly the same. The standard deviation of the differences is slightly worse for the Northern Hemisphere (from 1.3 ppm to 1.5 ppm) and slightly better for the Southern Hemisphere (from 1.3 ppm to 0.9 ppm). The annual increase, the seasonal cycle amplitude and the detrended correlation of the Northern Hemisphere are not changed significantly. The reason for the observed difference in the seasonal cycle amplitude can be an underestimation of the net ecosystem exchange (NEE) between the atmosphere and the biosphere in the CASA (Carnegie-Ames-Stanford Approach) biosphere model which is used by CarbonTracker (Yang et al., 2007; Schneising et al., 2012; Keppel-Aleks et al., 2012; Messerschmidt et al., 2012). For the Southern Hemisphere, the annual increase of WFMDv2.2 is also not changed significantly. However, the seasonal cycle amplitude is lower for WFMDv2.2 and agrees better with CarbonTracker compared to WFMDv2.1. The phase shift of the seasonal cycle of WFMDv2.1 shown by the detrended correlation of -0.19 was significantly improved for WFMDv2.2 shown by the detrended correlation of 0.72.

Overall, the SCIAMACHY WFM-DOAS v2.2 XCO_2 data product shows much better agreements with CarbonTracker compared to WFMDv2.1.

8 Summary and conclusions

We have presented an improved version (WFMDv2.2) of the SCIAMACHY WFM-DOAS XCO_2 retrieval algorithm. This algorithm utilises an improved cloud filtering and correction method using the 1.4 µm water vapour absorption and 0.76 µm O_2-A bands to identify and select cloud free scenes. A new SCIAMACHY XCO_2 data set covering the years 2003–2009 has been generated by using this new version. In order to validate the new XCO_2 data product, we used ground-based FTS observations from TCCON.

The validation showed a significant improvement of the new SCIAMACHY XCO_2 data product (v2.2) in comparison to the previous product (v2.1). For example, the large time dependent deviation from the FTS measurements at Darwin was reduced from a standard deviation of 4 ppm to 2 ppm. The monthly regional-scale scatter of the data (defined as standard deviation of all monthly quality filtered XCO_2 retrievals within a radius of 350 km around various locations) was also improved typically by a factor of about 1.5. Overall, the single measurement precision has been improved from 5.4 ppm for WFMDv2.1 to 3.8 ppm for WFMDv2.2, the monthly regional-scale precision has been improved from 2.1 ppm to 1.6 ppm, the regional-scale relative accuracy has been improved from 1.1 ppm to 0.8 ppm and the mean correlation has also been improved from 0.76 to 0.84.

In addition to the comparison with the limited number of TCCON sites, we also presented results of a comparison with NOAA's global CO_2 modelling and assimilation system CarbonTracker. The results of this comparison also showed significant improvements of the new XCO_2 data product especially over the Southern Hemisphere (e.g. a reduction of the phase shift between the SCIAMACHY and CarbonTracker XCO_2).

These results show that the improved cloud filtering and correction method of the new version of the SCIAMACHY WFM-DOAS retrieval algorithm successfully improves the SCIAMACHY XCO_2 data product. The new data

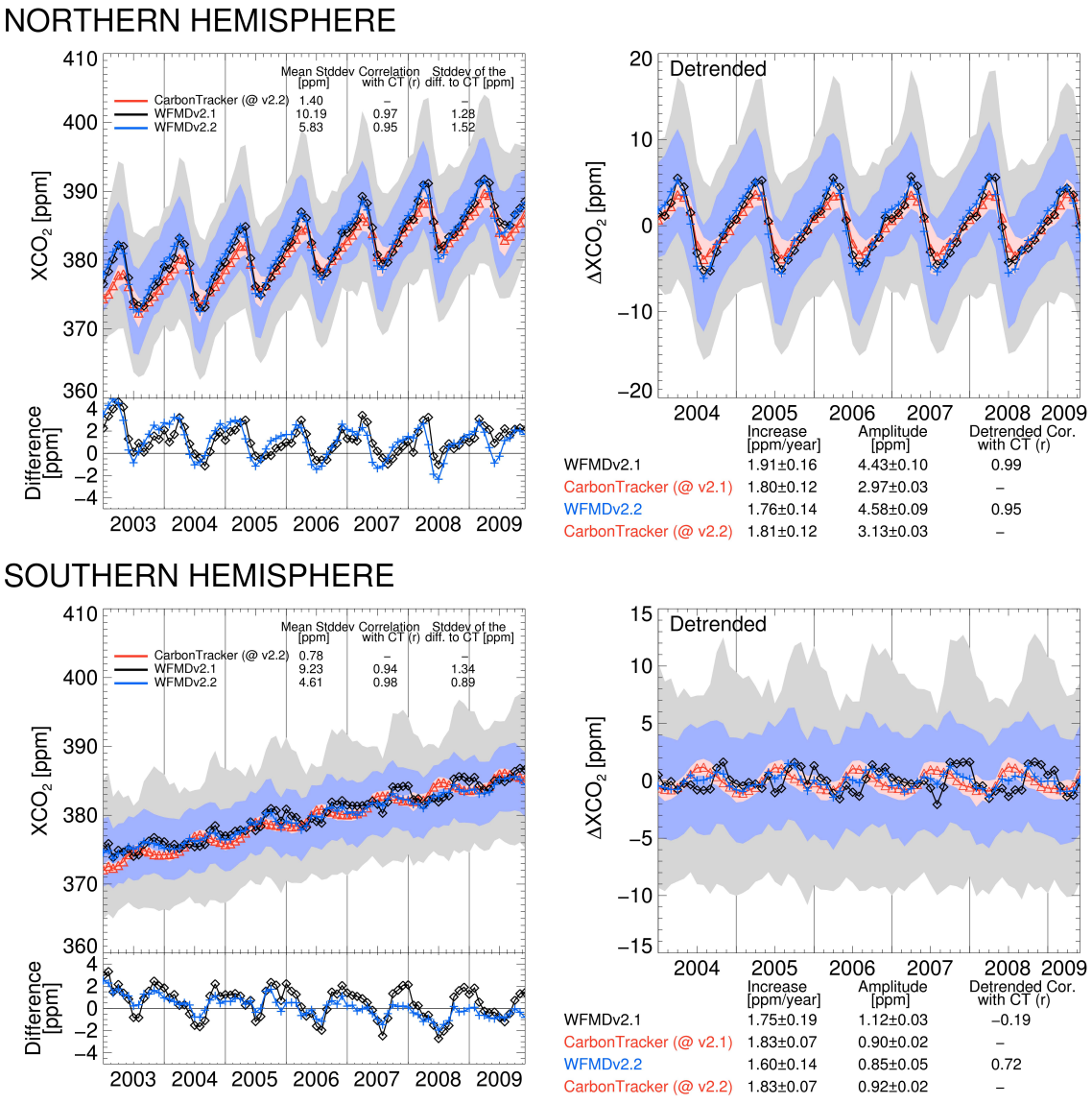

Fig. 9. Comparison of SCIAMACHY WFM-DOAS version 2.1 (WFMDv2.1) and 2.2 (WFMDv2.2) with CarbonTracker XCO_2 for the Northern (top) and Southern (bottom) Hemisphere for the years 2003–2009. CarbonTracker was sampled as WFMDv2.1 (@v2.1) for the comparison with WFMDv2.1 and sampled as WFMDv2.2 (@v2.2) for the comparison with WFMDv2.2. Top: The left panel shows the time series of monthly means of WFMDv2.1 (black diamonds), WFMDv2.2 (blue crosses) and CarbonTracker (red triangles) XCO_2 and the difference to CarbonTracker for the Northern Hemisphere. The shaded areas represent the monthly standard deviations of WFMDv2.1 (grey), WFMDv2.2 (light blue) and CarbonTracker (red). In addition, the averaged monthly standard deviation, the correlation with CarbonTracker and the standard deviation of the difference to CarbonTracker are shown. The right panel shows the detrended time series. Furthermore, the annual increase, the seasonal cycle amplitude and the detrended correlation (correlation between the detrended satellite time series and CarbonTracker) are shown. Bottom: as in top panels but for the Southern Hemisphere.

set is available on request from http://www.iup.uni-bremen.de/sciamachy/NIR_NADIR_WFM_DOAS/.

Acknowledgements. CarbonTracker version 2010 data were provided by NOAA ESRL, Boulder, Colorado, USA, via the website at http://carbontracker.noaa.gov. We thank ECMWF for providing the meteorological data. The TCCON data were obtained from the TCCON Data Archive, operated by the California Institute of Technology from the website at http://tccon.ipac.caltech.edu/. We further thank the two anonymous referees for their helpful and valuable comments. The research leading to the results presented in this manuscript has received funding from the European Union's Seventh Framework Programme (FP7) under Grant Agreements no. 212095 (CityZen) and 218793 (MACC), ESA (ADVANSE, CARBONGASES, GHG-CCI, SQWG), DLR (SADOS) and the University and the State of Bremen.

The Garmisch TCCON activities have been funded by the ESA GHG-CCI project via subcontract with the University of Bremen and by the EC within the INGOS project.

The Darwin and Wollongong TCCON sites are funded by NASA grants NAG5-12247 and NNG05-GD07G and the Australian Research Council, DP0879468 and LP0562346. We are grateful to the DOE ARM program for technical support in Darwin.

The Park Falls and Lamont TCCON stations are funded by NASA grants NNX11AG01G, NAG5-12247, NNG05-GD07G, and NASA's Orbiting Carbon Observatory Program. We are grateful to the DOE ARM program for technical support in Lamont and Jeff Ayers for technical support in Park Falls.

The TCCON site at Bialystok is financially supported by the Senate of Bremen and the EU projects IMECC and GEOmon. We acknowledge maintenance and logistical work provided by AeroMeteo Service (Bialystok) and RAMCES team at LSCE (Gif-sur-Yvette, France).

Edited by: T. von Clarmann

References

Barkley, M. P., Frieß, U., and Monks, P. S.: Measuring atmospheric CO_2 from space using Full Spectral Initiation (FSI) WFM-DOAS, Atmos. Chem. Phys., 6, 3517–3534, doi:10.5194/acp-6-3517-2006, 2006a.

Barkley, M. P., Monks, P. S., Hewitt, A. J., Machida, T., Desai, A., Vinnichenko, N., Nakazawa, T., Yu Arshinov, M., Fedoseev, N., and Watai, T.: Assessing the near surface sensitivity of SCIAMACHY atmospheric CO_2 retrieved using (FSI) WFM-DOAS, Atmos. Chem. Phys., 7, 3597–3619, doi:10.5194/acp-7-3597-2007, 2007.

Basu, S., Houweling, S., Peters, W., Sweeney, C., Machida, T., Maksyutov, S., Patra, P. K., Saito, R., Chevallier, F., Niwa, Y., Matsueda, H., and Sawa, Y.: The seasonal cycle amplitude of total column CO_2: factors behind the model-observation mismatch, J. Geophys. Res., 116, D23306, doi:10.1029/2011JD016124, 2011.

Bösch, H., Toon, G. C., Sen, B., Washenfelder, R. A., Wennberg, P. O., Buchwitz, M., de Beek, R., Burrows, J. P., Crisp, D., Christi, M., Connor, B. J., Natraj, V., and Yung, Y. L.: Space-based near-infrared CO_2 measurements: testing the Orbiting Carbon Observatory retrieval algorithm and validation concept using SCIAMACHY observations over Park Falls, Wisconsin, J. Geophys. Res., 111, D23302, doi:10.1029/2006JD007080, 2006.

Bösch, H., Baker, D., Connor, B., Crisp, D., and Miller, C.: Global characterization of CO_2 column retrievals from shortwave-infrared satellite observations of the Orbiting Carbon Observatory-2 mission, Remote Sens., 3, 270–304, doi:10.3390/rs3020270, 2011.

Bovensmann, H., Burrows, J. P., Buchwitz, M., Frerick, J., Noël, S., Rozanov, V. V., Chance, K. V., and Goede, A.: SCIAMACHY – mission objectives and measurement modes, J. Atmos. Sci., 56, 127–150, 1999.

Bovensmann, H., Buchwitz, M., Burrows, J. P., Reuter, M., Krings, T., Gerilowski, K., Schneising, O., Heymann, J., Tretner, A., and Erzinger, J.: A remote sensing technique for global monitoring of power plant CO_2 emissions from space and related applications, Atmos. Meas. Tech., 3, 781–811, doi:10.5194/amt-3-781-2010, 2010.

Buchwitz, M. and Burrows, J. P.: Retrieval of CH_4, CO, and CO_2 total column amounts from SCIAMACHY near-infrared nadir spectra: retrieval algorithm and first results, in: Remote Sensing of Clouds and the Atmosphere VIII, edited by: Schäfer, K. P., Comèron, A., Carleer, M. R., and Picard, R. H., Proc. SPIE, 5235, 375–388, 2004.

Buchwitz, M., Rozanov, V. V., and Burrows, J. P.: A near-infrared optimized DOAS method for the fast global retrieval of atmospheric CH_4, CO, CO_2, H_2O, and N_2O total column amounts from SCIAMACHY Envisat-1 nadir radiances, J. Geophys. Res., 105, 15231–15245, 2000.

Buchwitz, M., de Beek, R., Noël, S., Burrows, J. P., Bovensmann, H., Schneising, O., Khlystova, I., Bruns, M., Bremer, H., Bergamaschi, P., Körner, S., and Heimann, M.: Atmospheric carbon gases retrieved from SCIAMACHY by WFM-DOAS: version 0.5 CO and CH_4 and impact of calibration improvements on CO_2 retrieval, Atmos. Chem. Phys., 6, 2727–2751, doi:10.5194/acp-6-2727-2006, 2006.

Buchwitz, M., Schneising, O., Burrows, J. P., Bovensmann, H., Reuter, M., and Notholt, J.: First direct observation of the atmospheric CO_2 year-to-year increase from space, Atmos. Chem. Phys., 7, 4249–4256, doi:10.5194/acp-7-4249-2007, 2007.

Burrows, J. P., Hölzle, E., Goede, A. P. H., Visser, H., and Fricke, W.: SCIAMACHY – Scanning Imaging Absorption Spectrometer for Atmospheric Chartography, Acta Astronaut., 35, 445–451, 1995.

Butz, A., Hasekamp, O. P., Frankenberg, C., and Aben, I.: Retrievals of atmospheric CO_2 from simulated space-borne measurements of backscatteres near-infrared sunlight: accounting for aerosol effects, Appl. Opt., 48, 3322–3336, 2009.

Chevallier, F., Bréon, F.-M., and Rayner, P. J.: Contribution of the Orbiting Carbon Observatory to the estimation of CO_2 sources and sinks: theoretical study in a variational data assimilation framework, J. Geophys. Res., 112, D09307, doi:10.1029/2006JD007375, 2007.

Crisp, D., Atlas, R. M., Bréon, F.-M., Brown, L. R., Burrows, J. P., Ciais, P., Connor, B. J., Doney, S. C., Fung, I. Y., Jacob, D. J., Miller, C. E., O'Brien, D., Pawson, S., Randerson, J. T., Rayner, P., Salawitch, R. S., Sander, S. P., Sen, B., Stephens, G. L., Tans, P. P., Toon, G. C., Wennberg, P. O., Wofsy, S. C., Yung, Y. L., Kuang, Z., Chudasama, B., Sprague, G., Weiss, P., Pollock, R., Kenyon, D., and Schroll, S.: The Orbiting Carbon Observatory (OCO) mission, Adv. Space Res., 34, 700–709, 2004.

Gao, B.-C., Goetz, A. F. H., and Wiscombe, W. J.: Cirrus cloud detection from airborne imaging spectromter data using the 1.38 µm water vapor band, Geophys. Res. Lett., 20, 301–304, 1993.

Heymann, J., Schneising, O., Reuter, M., Buchwitz, M., Rozanov, V., Bovensmann, H., and Burrows, J. P.: SCIAMACHY WFM-DOAS XCO_2 : Comparison with CarbonTracker XCO_2 focusing on aerosols and thin clouds, Atmos. Meas. Tech., 5, 1935–1952, doi:10.5194/amt-5-1935-2012, 2012.

Houweling, S., Breon, F.-M., Aben, I., Rödenbeck, C., Gloor, M., Heimann, M., and Ciais, P.: Inverse modeling of CO_2 sources and sinks using satellite data: a synthetic inter-comparison of measurement techniques and their performance as a function of space and time, Atmos. Chem. Phys., 4, 523–538, doi:10.5194/acp-4-523-2004, 2004.

Houweling, S., Hartmann, W., Aben, I., Schrijver, H., Skidmore, J., Roelofs, G.-J., and Breon, F.-M.: Evidence of systematic errors in SCIAMACHY-observed CO_2 due to aerosols, Atmos. Chem. Phys., 5, 3003–3013, doi:10.5194/acp-5-3003-2005, 2005.

Keppel-Aleks, G., Wennberg, P. O., Washenfelder, R. A., Wunch, D., Schneider, T., Toon, G. C., Andres, R. J., Blavier, J.-F., Connor, B., Davis, K. J., Desai, A. R., Messerschmidt, J., Notholt, J., Roehl, C. M., Sherlock, V., Stephens, B. B., Vay, S. A., and Wofsy, S. C.: The imprint of surface fluxes and transport on variations in total column carbon dioxide, Biogeosciences, 9, 875–891, doi:10.5194/bg-9-875-2012, 2012.

Kuze, A., Suto, H., Nakajima, M., and Hamazaki, T.: Thermal and near infrared sensor for carbon observation Fourier-transform spectrometer on the Greenhouse Gases Observing Satellite for greenhouse gases monitoring, Appl. Optics, 48, 6716–6733, 2009.

Messerschmidt, J., Parazoo, N., Deutscher, N. M., Roehl, C., Warneke, T., Wennberg, P. O., and Wunch, D.: Evaluation of atmosphere-biosphere exchange estimations with TCCON measurements, Atmos. Chem. Phys. Discuss., 12, 12759–12800, doi:10.5194/acpd-12-12759-2012, 2012.

Miller, C. E., Crisp, D., DeCola, P. L., Olsen, S. C., Randerson, J. T., Michalak, A. M., Alkhaled, A., Rayner, P., Jacob, D. J., Suntharalingam, P., Jones, D. B. A., Denning, A. S., Nicholls, M. E., Doney, S. C., Pawson, S., Boesch, H., Connor, B. J., Fung, I. Y., O'Brien, D., Salawitch, R. J., Sander, S. P., Sen, B., Tans, P., Toon, G. C., Wennberg, P. O., Wofsy, S. C., Yung, Y. L., and Law, R. M.: Precision requirements for space-based XCO_2 data, J. Geophys. Res., 112, D10314, doi:10.1029/2006JD007659, 2007.

Morino, I., Uchino, O., Inoue, M., Yoshida, Y., Yokota, T., Wennberg, P. O., Toon, G. C., Wunch, D., Roehl, C. M., Notholt, J., Warneke, T., Messerschmidt, J., Griffith, D. W. T., Deutscher, N. M., Sherlock, V., Connor, B., Robinson, J., Sussmann, R., and Rettinger, M.: Preliminary validation of column-averaged volume mixing ratios of carbon dioxide and methane retrieved from GOSAT short-wavelength infrared spectra, Atmos. Meas. Tech., 4, 1061–1076, doi:10.5194/amt-4-1061-2011, 2011.

O'Dell, C. W., Connor, B., Bösch, H., O'Brien, D., Frankenberg, C., Castano, R., Christi, M., Eldering, D., Fisher, B., Gunson, M., McDuffie, J., Miller, C. E., Natraj, V., Oyafuso, F., Polonsky, I., Smyth, M., Taylor, T., Toon, G. C., Wennberg, P. O., and Wunch, D.: The ACOS CO_2 retrieval algorithm - Part 1: Description and validation against synthetic observations, Atmos. Meas. Tech., 5, 99–121, doi:10.5194/amt-5-99-2012, 2012.

Oshchepkov, S., Bril, A., and Yokota, T.: PPDF-based method to account for atmospheric light scattering in observations of carbon dioxide from space, J. Geophys. Res.-Atmos., 113, D23210, doi:10.1029/2008JD010061, 2008.

Peters, W., Jacobson, A. R., Sweeney, C., Andrews, A. E., Conway, T. J., Masarie, K., Miller, J. B., Bruhwiler, L. M. P., Petron, G., Hirsch, A. I., Worthy, D. E. J., van der Werf, G. R., Randerson, J. T., Wennberg, P. O., Krol, M. C., and Tans, P. P.: An atmospheric perspective on North American carbon dioxide exchange: CarbonTracker, Proc. Natl. Acad. Sci. USA, 104, 18925–18930, doi:10.1073/pnas.0708986104, 2007.

Rayner, P. J. and O'Brien, D. M.: The utility of remotely sensed CO_2 concentration data in surface inversions, Geophys. Res. Lett., 28, 175–178, 2001.

Reuter, M., Bovensmann, H., Buchwitz, M., Burrows, J. P., Connor, B. J., Deutscher, N. M., Griffith, D. W. T., Heymann, J., Keppel-Aleks, G., Messerschmidt, J., Notholt, J., Petri, C., Robinson, J., Schneising, O., Sherlock, V., Velazco, V., Warneke, T., Wennberg, P. O., and Wunch, D.: Retrieval of atmospheric CO_2 with enhanced accuracy and precision from SCIAMACHY: Validation with FTS measurements and comparison with model results, J. Geophys. Res., 116, D04301, doi:10.1029/2010JD015047, 2011.

Rodgers, C. D.: Inverse Methods for Atmospheric Sounding: Theory and Practice, World Scientific Publishing, Singapore, 2000.

Saitoh, N., Imasu, R., Ota, Y., and Niwa, Y.: CO_2 retrieval algorithm for the thermal infrared spectra of the Greenhouse Gases Observing Satellite: potential of retrieving CO_2 vertical profile from high-resolution FTS sensor, J. Geophys. Res., 114, D17305, doi:10.1029/2008JD011500, 2009.

Schneising, O., Buchwitz, M., Burrows, J. P., Bovensmann, H., Reuter, M., Notholt, J., Macatangay, R., and Warneke, T.: Three years of greenhouse gas column-averaged dry air mole fractions retrieved from satellite – Part 1: Carbon dioxide, Atmos. Chem. Phys., 8, 3827–3853, doi:10.5194/acp-8-3827-2008, 2008.

Schneising, O., Buchwitz, M., Reuter, M., Heymann, J., Bovensmann, H., and Burrows, J. P.: Long-term analysis of carbon dioxide and methane column-averaged mole fractions retrieved from SCIAMACHY, Atmos. Chem. Phys., 11, 2863–2880, doi:10.5194/acp-11-2863-2011, 2011.

Schneising, O., Bergamaschi, P., Bovensmann, H., Buchwitz, M., Burrows, J. P., Deutscher, N. M., Griffith, D. W. T., Heymann, J., Macatangay, R., Messerschmidt, J., Notholt, J., Rettinger, M., Reuter, M., Sussmann, R., Velazco, V. A., Warneke, T., Wennberg, P. O., and Wunch, D.: Atmospheric greenhouse gases retrieved from SCIAMACHY: comparison to ground-based FTS measurements and model results, Atmos. Chem. Phys., 12, 1527–1540, doi:10.5194/acp-12-1527-2012, 2012.

Stephens, B. B., Gurney, K. R., Tans, P. P., Sweeney, C., Peters, W., Bruhwiler, L., Ciais, P., Ramonet, M., Bousquet, P., Nakazawa, T., Aoki, S., Machida, T., Inoue, G., Vinnichenko, N., Lloyd, J., Jordan, A., Heimann, M., Shibistova, O., Langenfelds, R. L., Steele, L. P., Francey, R. J., and Denning, A. S.: Weak northern and strong tropical land carbon uptake from vertical profiles of atmospheric CO_2, Science, 316, 1732–1735, doi:10.1126/science.1137004, 2007.

Tilstra, L. G., de Graaf, M., Aben, I., and Stammes, P.: Analysis of 5 years of SCIAMACHY absorbing aerosol index data, Proceedings ENVISAT Symposium, Montreux, Switzerland, ESA Special Publication SP-636, 2007.

Wunch, D., Toon, G. C., Blavier, J., Washenfelder, R. A., Notholt, J., Connor, B. J., Griffith, D. W. T., Sherlock, V., and Wennberg, P. O.: The total carbon column observing network, Philos. T. Roy. Soc. A, 369, 2087–2112, doi:10.1098/rsta.2010.0240, 2011.

Yang, Z., Washenfelder, R. A., Keppel-Aleks, G., Krakauer, N. Y., Randerson, J. T., Tans, P. P., Sweeney, C., and Wennberg, P. O.: New constraints on Northern Hemisphere growing season net flux, Geophys. Res. Lett., 34, L12807, doi:10.1029/2007GL029742, 2007.

Yokota, T., Oguma, H., Morino, I., and Inoue, G.: A nadir looking SWIR sensor to monitor CO_2 column density for Japanese GOSAT project, Proceedings of the twenty-fourth international symposium on space technology and science, Miyazaki: Japan Society for Aeronautical and Space Sciences and ISTS, 887–889, 2004.

Yoshida, J., Kawashima, T., Ishida, J., Kuze, A., Suto, H., Shiomi, K., and Nakajima, M.: GOSAT/TANSO: Instrument Design and Level 1 Product Processing Algorithms, Fourier Transform Spectroscopy, OSA Technical Digest (CD) (Optical Society of America, 2011), paper JPDP1, available at: http://www.opticsinfobase.org/abstract.cfm?URI=FTS-2011-JPDP1 (last access: June 2012), 2011a.

Yoshida, Y., Ota, Y., Eguchi, N., Kikuchi, N., Nobuta, K., Tran, H., Morino, I., and Yokota, T.: Retrieval algorithm for CO_2 and CH_4 column abundances from short-wavelength infrared spectral observations by the Greenhouse gases observing satellite, Atmos. Meas. Tech., 4, 717–734, doi:10.5194/amt-4-717-2011, 2011b.